

RESEARCH

Open Access



# Numerical Simulation Study on the Seismic Performance of Prefabricated Fiber-Reinforced Concrete Beam–Column Joints With Grouted Sleeve Connections

Mei-Ling Zhuang<sup>1,2,3</sup>, Jinsheng Cheng<sup>4</sup>, Dongsong Fei<sup>4</sup>, Chuanzhi Sun<sup>5\*</sup>, Zhenbo Wang<sup>6</sup>, Baodong Chen<sup>6</sup> and Yan Qiao<sup>4,5</sup>

## Abstract

Based on the available experimental data, fiber models for four prefabricated fiber-reinforced concrete beam–column joint specimens with grouted sleeve connections are first developed in OpenSees software. Then, the simulated seismic performance of the specimens is compared with the experimental results. Finally, the effects of axial load ratio and shear-to-span ratio on the seismic performance of the specimens are further investigated numerically. The results indicate that Concrete02 material model and Reinforcing Steel material model can accurately simulate the constitutive relationship of concrete and reinforcing steel, respectively; the beam–column joint elements can accurately simulate different damage behaviors of the joint zone. Fiber-reinforced concrete can significantly improve the seismic performance of the specimens. The relative errors of the simulated seismic performance indexes are about 15%. It is recommended that the optimum value of shear-to-span ratio for prefabricated FRC BCJs is 2.0–2.5. The effect of axial load ratio on the seismic behavior of PBCJs-CM is very small, and can be negligible in the case that the prefabricated FRC BCJs has a moderate value of shear-to-span ratio. The fiber model developed in this article can provide a numerical simulation basis for subsequent studies of prefabricated fiber-reinforced concrete beam–column joint specimens with grouted sleeve connections.

**Keywords** Prefabricated concrete frame joint, Fiber-reinforced concrete, Fiber model, Axial load ratio, Shear-to-span

Journal information: ISSN 1976-0485 / eISSN 2234-1315.

\*Correspondence:

Chuanzhi Sun  
schzh\_xzh@163.com

<sup>1</sup> School of Transportation and Civil Engineering, Nantong University,  
Nantong 226019, China

<sup>2</sup> School of Civil Engineering, Shandong University, Jinan 250061, China

<sup>3</sup> Water Resources Research Institute of Shandong Province, Jinan 250013,  
China

<sup>4</sup> Suqian City Urban Construction Investment (Group) Co. Ltd,  
Suqian 223800, China

<sup>5</sup> School of Civil Engineering and Architecture, Suqian College,  
Suqian 223800, China

<sup>6</sup> College of Civil Engineering, Nanjing Tech University, Nanjing 211800,  
China

## 1 Introduction

The assembled building realizes standardized design, factory production, assembled construction and information management. Its mass production method can largely reduce the generation of construction waste and energy consumption during construction, as well as reduce carbon emissions in the whole life cycle of the building, which is in line with the concept of green ecological development and promotes the sustainable development of the construction industry (Li et al., 2022; MOHURD (Ministry of Housing and Urban–Rural Development of the People’s Republic of China) 2014a; ; ; MOHURD (Ministry of Housing and Urban–Rural Development of the People’s Republic of China) 2014b;

Ministry of Housing & Urban–Rural Development of Jiangsu Province, 2017; Ministry of Housing & Urban–Rural Development of Jiangsu Province. Technical specification for assembled monolithic concrete structure, 2014). Therefore, prefabricated-reinforced concrete (PRC) structures have been widely studied in recent years (Parastesh et al., 2014; Girgin et al., 2017; Kurama et al., 2018). At present, several connection methods have been proposed for beam–column joints (BCJs), such as sleeve cold extrusion connection, slurry anchor connection, and grouted sleeve connection. Among them, grouted sleeve connections are most commonly used.

The seismic performance of BCJs is a key issue limiting the development of PRC structures (Nadir et al., 2021; Xue et al., 2021). The seismic performance of PRC BCJs with wet connections is usually closer to that of cast-in-place concrete (CPRC) BCJs (Guan et al., 2019; Xia et al., 2020). Experimental investigations have shown that the displacement ductility, energy dissipation capacity and shear resistance capacity of FRC members are good. Dangwal and Singh (Dangwal & Singh, 2023) proved experimentally that high strength fiber-reinforced concrete (HSFRC) can improve the bearing capacity, stiffness and energy dissipation capacity of BCJs. Qian et al. (Qian et al., 2023) investigated an innovative re-centering shape memory alloy bars and engineered cementitious composites (SMA-ECC) based prefabricated beam–column joints and found that the specimen joints can undergo large displacement with superior self-centering and energy dissipation capacities. Zhuang et al. (Zhuang et al., 2022a) studied the drift ratio limits of PVA fiber-reinforced concrete columns under different performance levels through the quasi-static tests. The experimental results indicated that the PVA fiber can improved the seismic performance of reinforced concrete columns. PVA fiber not only can improve dynamic and material properties of fiber-reinforced concrete (Noushini et al., 2013, 2015), and also can improve the ductility and damping characteristics of reinforced concrete members (Fischer & Li, 2002). The performance enhancement in terms of stiffness, strength, ductility, and energy absorption capacity, which could be achieved by replacing concrete with the high-performance material ECC, different fiber-reinforced concrete (Gencturk et al., 2013; Gul et al., 2023; Parra-Montesinos & Chomprea, 2017; Saghafi et al., 2021; Said & Razak, 2016; Suryanto et al., 2022). In 2023, Sun et al. first investigated the seismic performance of prefabricated concrete and prefabricated fiber-reinforced concrete (FRC) BCJs by the quasi-static tests (Sun et al., 2023a). In reference (Sun et al., 2023a), the design and fabrication of the test specimens were given in detail. The prefabricated beams were connected

by the anchorage of the bottom reinforcement, while the prefabricated columns were connected using grouted sleeves (Sun et al., 2023a). Concrete or FRC was poured in the core zone of the joint, as shown in Fig. 1. The experimental results proved that FRC can improve the seismic behaviors of prefabricated BCJs, which was consistent with the conclusion in the references (Dangwal & Singh, 2023; Noushini et al., 2013, 2015; Parra-Montesinos & Chomprea, 2017; Saghafi et al., 2021; Zhuang et al., 2022a).

Combined with experiment investigations, numerical methods are important for predicting the structural response of buildings. So far, many finite-element models (FEMs) have been developed to simulate the seismic behavior of reinforced concrete (RC) members. Among them, fiber models are computationally inexpensive, easy to model, and have better accuracy (Zhuang et al., 2022b). Prefabricated joints are subjected to complex stresses and are prone to the formation of structural defects that lead to stress concentrations. In practical engineering, while the entire structure is often in an elastic phase, the joints may have transitioned to a plastic phase and suffered severe damage. This can eventually lead to structural failure. Therefore, it is crucial to focus on joint analysis for RC frame structures in numerical modeling. How to effectively reflect the seismic performance of prefabricated FRC BCJs using numerical simulation methods is very important to promote the development of prefabricated FRC BCJs. Paulay (Paulay, 1989) pointed out that the deformation of BCJs mainly consisted of shear deformation of joint shear blocks and corner deformation at the beam–column intersections. Pantazopoulou and Bonacci (Pantazopoulou & Bonacci, 1994) pointed out that the slip of reinforcement causes blocked load transfer at the intersection and further leads to damage of the joint shear block. Lowes and Altoontash (Lowes & Altoontash, 2003) proposed a beam–column

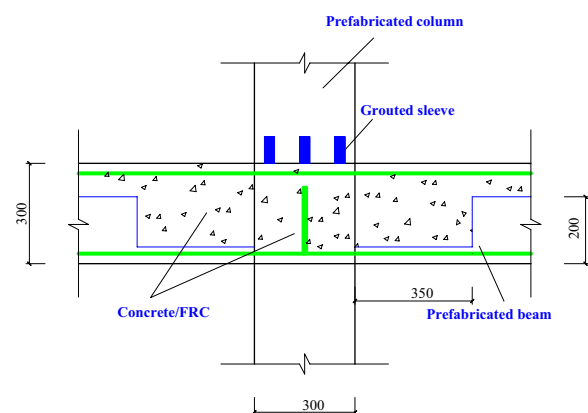


**Fig. 1** Prefabricated concrete or FRC BCJs (Sun et al., 2023a)

joint element, which was then modified by N-Mitra (Mitra, 2007). It consists of three components to simulate the different damage behaviors of BCJs. The shear panel component is located in the middle of the beam–column joint element and is used to simulate the shear behavior of strength and stiffness degradation of the joint core zone under shear damage. Under low-cycle reciprocating loads, bond-slip occurs between the reinforcement and concrete, which in turn leads to pinching of the hysteresis loops and has a significant impact on the load–displacement curve. Using the stress-slip relationship for reinforcement proposed by Eligehausen and Hawkins, a reinforcement bond-slip constitutive model, Bar-slip, was developed in OpenSees software (Eligehausen et al., 1982; Hawkins et al., 1982). It analyzes the effect of slip on the connection by considering the effects of concrete strength, reinforcement material properties and degree of anchorage. There are some numerical simulation investigations on the seismic performance of PRC BCJs. Paudel, Tanapornraweekit, and Tangtermsirikul (Paudel et al., 2022) evaluated the seismic behavior of prefabricated U BCJs with good accuracy using LS-DYNA finite-element software. Xia et al., (2023) established a refined finite-element model using ABAQUS software. C3D8R solid elements was employed for the concrete, grouting material, longitudinal steel bar, and sleeve, while T3D2 truss elements are used for the stirrup and steel bar cage of the base. The bond slip between the steel bar and concrete and the steel bar and grouting material was simulated using the cohesive model. The numerical relative errors of the established finite-element models were within 15%. However, there is no knowledge on the numerical study of the seismic performance of prefabricated FRC BCJs with grouted sleeve connections. In addition, the suitability of the existing constitutive models for the prefabricated FRC BCJs with grouted sleeve connections needs to be verified by numerical simulation investigations.

To further promote the development of FRC in prefabricated BCJs, the seismic performance of

prefabricated FRC BCJs is investigated numerically in this article. One prefabricated concrete and three prefabricated FRC BCJs are selected from references (Sun et al., 2023a, 2023b). The FEMs of the prefabricated specimens are established using OpenSees software. The simulated seismic performance of the specimens is compared with the experimental results in reference (Sun et al., 2023a). Based on this, the effects of axial load ratio and shear-to-span ratio on the seismic behavior of the precast BCJs are further investigated numerically.

## 2 Quasi-Static Test Programs and Numerical Models

### 2.1 Overall Design of Quasi-Static Test Programs

One prefabricated concrete and three prefabricated FRC BCJs from reference (Sun et al., 2023a, 2023b) are selected for the numerical simulation. Specimen PRC1 is a PRC BCJs. Specimen PFRC1 and PFRC2 are PRC BCJs reinforced with PVA fibers (see Fig. 2a). Specimen PFRC3 is a PRC beam–column joint (BCJ) reinforced with steel fibers (see Fig. 2b). There are no stirrups in the core zone of specimens PFRC2, but there are stirrups in the core zone of the other three specimens. Tables 1 and 2 list the mix ratios of PVA and steel FRC. Fig. 3 shows the design details of specimens PRC1, PFRC1 and PFRC3. In the joint core zone, the design parameters of the four prefabricated BCJs are designed in Table 3. The mechanical properties of concrete, PVA concrete and Steel FRC can be seen in Tables 4 and 5 (Sun et al., 2023a, 2023b). The mechanical properties of steel bars are described in Fig. 4.

### 2.2 Numerical Models of Prefabricated BCJs

#### 2.2.1 Constitutive Models of Materials

OpenSees software provides a large number of material models for users to choose from. Among them, uniaxial materials can establish force–displacement



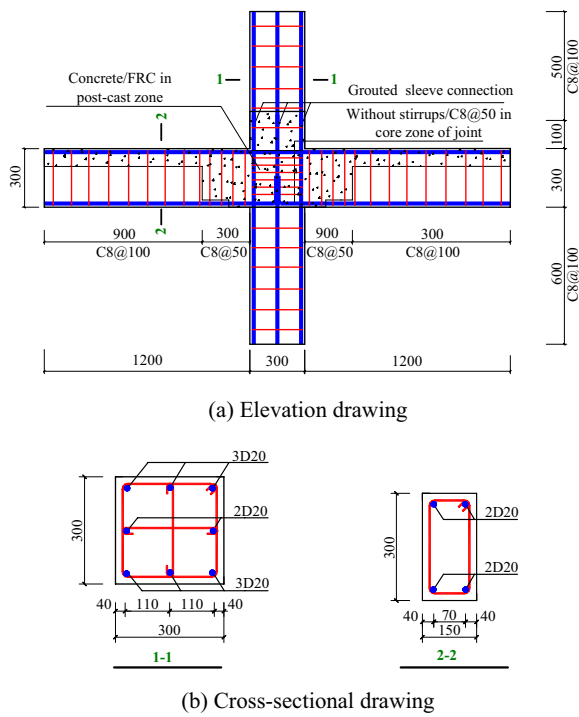
Fig. 2 Photos of fibers

Table 1 Mix ratio of PVA fiber-reinforced concrete

Cement (kg/m <sup>3</sup> )	Sand (kg/m <sup>3</sup> )	Stone (kg/m <sup>3</sup> )	Water (kg/m <sup>3</sup> )	Water reducing (kg/m <sup>3</sup> )	Volume content of fibers (%)
400	753	1080	165	5.4	0.30

Table 2 Mix ratio of steel fiber-reinforced concrete

Cement (kg/m <sup>3</sup> )	Sand (kg/m <sup>3</sup> )	Stone (kg/m <sup>3</sup> )	Water (kg/m <sup>3</sup> )	Water reducing (kg/m <sup>3</sup> )	Volume content of fibers (%)
400	753	1080	165	5.4	1.00



**Fig. 3** Details of prefabricated BCJs (Sun et al., 2023a)

relationship, which have the advantages of clear theoretical logic, simple working principle, and easy determination of material model parameters. Based on the modified Kent-Park concrete model, Concrete02 constitutive model was proposed (see Fig. 4), which effectively takes into account the tensile properties of concrete (Scott et al., 1982), thus enabling the simulation of the hysteretic performance of confined concrete in tension and compression. The introduction of the reinforcement coefficient  $K$  also takes into account the strengthening effect of stirrups on the strength and ductility of the concrete in the core zone, which can more accurately simulate the constitutive relationship of the concrete. When subjected to tension, the skeleton curve of the Concrete02 constitutive model is a bi-fold model, i.e., elastic rising section and linear falling section; when subjected to compression, the

**Table 4** Compressive strength of concrete and FRC

Concrete grade	$V_c$ (%)	$f$ (MPa)			$f'$ (MPa)
		Specimen 1	Specimen 2	Specimen 3	
C35	0	36.10	35.57	35.02	35.56
C35	0.1	36.02	35.01	37.10	36.04
C35	0.2	37.58	38.45	34.88	36.97
C35	0.3	38.85	39.89	36.01	38.25
C35	0.4	36.41	37.08	35.55	36.35

Note:  $f$  is cub compressive strength;  $f'$  is the average of cub compressive strengths

**Table 5** Compressive strength of steel FRC

Concrete grade	$V_c$ (%)	$f$ (MPa)			$f'$ (MPa)
		Specimen 1	Specimen 2	Specimen 3	
C35	0.5	35.02	35.56	37.21	35.93
C35	0.75	37.58	34.89	38.45	37.42
C35	1.0	40.11	38.58	36.54	38.41

skeleton curve of Concrete02 constitutive model is based on Kent-Park model, which consists of 3 parts: parabolic rising section ( $\epsilon_c < \epsilon_0$ ), oblique linear falling section ( $\epsilon_0 \leq \epsilon_c \leq \epsilon_{0.2}$ ), and flat linear residual section ( $\epsilon_0 \leq \epsilon_c \leq \epsilon_{0.2}$ ). When  $\epsilon_c < \epsilon_0$ , the equation of the skeleton curve is

$$\sigma_c = kf'_c \left[ \frac{2\epsilon_c}{\epsilon_0} - \left( \frac{\epsilon_c}{\epsilon_0} \right)^2 \right] \quad (1)$$

When  $\epsilon_0 \leq \epsilon_c \leq \epsilon_{0.2}$ , the equation of the skeleton curve is

$$\sigma_c = kf[1 - Z_m(\epsilon_c - \epsilon_0)] \quad (2)$$

When  $\epsilon_0 \leq \epsilon_c \leq \epsilon_{0.2}$ , the equation of the skeleton curve is

**Table 3** Design parameters of prefabricated BCJs in the joint core zone

Specimen No	Concrete or FRC	$V_c$ (%)	Axial load ratio ( $n$ )	Spacing of stirrups
PRC1 (Sun et al., 2023a)	C35	0	0.15	50
PFRC1 (Sun et al., 2023b)	PVA FRC	0.30	0.15	50
PFRC2 (Sun et al., 2023a)	PVA FRC	0.30	0.15	No stirrups
PFRC3 (Sun et al., 2023a)	Steel FRC	1.00	0.15	50

Note:  $V_c$  is volume content of fibers

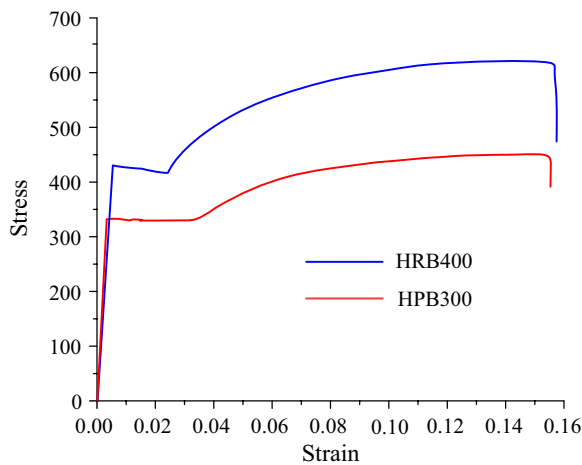


**Fig. 4** Stress–strain curves of steel bars under static tension

$$\sigma_c = 0.2f'_c \tag{3}$$

Equations (4, 5 and 6) show the corresponding equations for the parameters in Eqs. (1, 2 and 3):

$$\varepsilon_0 = 0.002k \tag{4}$$

$$k = 1 + \frac{\rho_s f_{yk}}{f'_c} \tag{5}$$

$$Z_m = 0.5 \left[ \frac{3 + 0.29f'_c}{145f'_c - 1000} + 0.75\rho_s \sqrt{\frac{h'}{s_h} - \varepsilon_0} \right] \tag{6}$$

In the above equations,  $\varepsilon_0$  is the strain corresponding to the peak load of the concrete;  $\varepsilon_{0.2}$  The strain corresponding to the decrease of concrete stress to 20% of the peak load;  $k$  is the reinforcement coefficient of the stirrup;  $Z_m$  is the slope of the residual segment of the straight line;  $\rho_s$  is the volume ratio of reinforcement;  $f_{yk}$  is the yield strength of the stirrup;  $f'_c$  is the compressive strength of cylindrical concrete;  $h'$  the width of the concrete in the core zone;  $s_h$  is the spacing between the stirrups.

Reinforcing steel constitutive model (see Fig. 5) is used as the constitutive model for reinforcement. The reinforcing steel constitutive model is based on the Chang–Mander constitutive model (Chang & Mander, 1994), while the buckling model of reinforcement (Gomes–Appleton model (Gomes & Appleton, 1997) and Dhakal–Maekawa model (Maekawa & Dhakal, 2002)) and fatigue damage model [Coffin–Manson model (Coffin, 1954; Manson, 1953)] are introduced. In this article, Dhakal–Maekawa buckling model is used

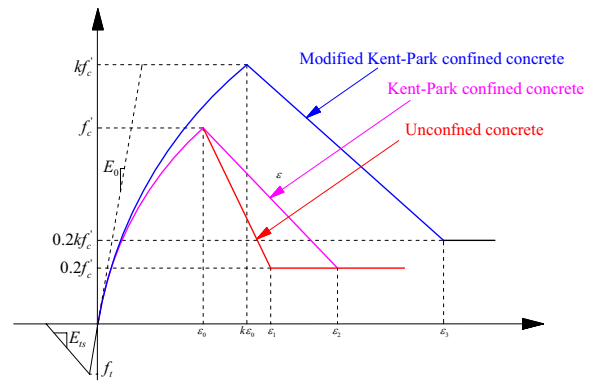


**Fig. 5** Stress–strain curves of Concrete02 constitutive mode under monotonic loading

to simulate buckling of compressed steel bars (Zhuang et al., 2022b). The Coffin–Manson model is used to simulate the adverse effects of the low-cycle fatigue accumulation damage of steel bars (Zhuang et al., 2022b). It has three parameters, namely, the strength degradation parameter  $C_d$ , the fatigue damage parameter  $C_f$  and the fatigue damage index  $\alpha_2$ . According to the previous study in reference (Zhang et al., 2016), the three parameters in the Coffin–Manson model can be obtained. In Fig. 6,  $f_y$ ,  $f_u$  are the yield strength and ultimate strength of the reinforcement, respectively;  $\varepsilon_{sh}$  is the starting point strain of the reinforcement and  $\varepsilon_u$  is

the strain of the reinforcement corresponding to  $f_u$ ;  $E_s$  is the initial modulus of elasticity of reinforcement;  $E_{sh}$  is the starting point modulus of the reinforcement.

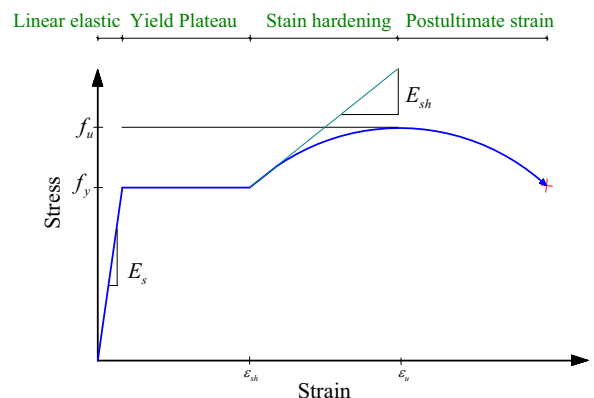
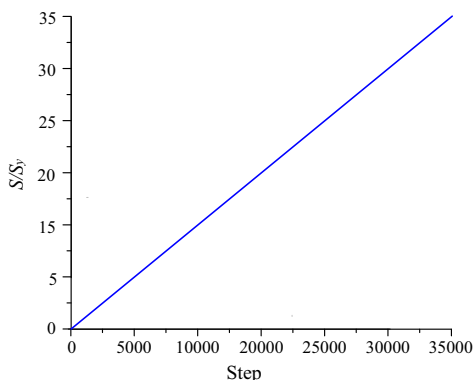


**Fig. 6** Stress–strain curve of Reinforcing steel constitutive model under monotonic loading

There are differences in construction quality, curing conditions and methods between cast-in concrete and post-cast zone concrete. The bond-slip between reinforcing steel and concrete is susceptible to the effects of greater reinforcement slippage in the BCJs. The Bond-SP01 constitutive model (Zhuang et al., 2022b) is chosen to simulate the bond-slip effect of reinforcement steel at the end of the beam and column, and the grouted sleeve connection. It has 6 parameters, i.e., yield strength  $f_y$ , slip at yield  $S_y$ , slip at failure  $S_u$ , intensification factor at the initial intensification phase  $b$  and hysteresis factor  $R$ . Zhao and Sritharan (Zhao & Sritharan, 2007) calculated and analyzed a large amount of pull-out test data to obtain a fitting formula for  $S_y$ , and recommended ranges for parameters  $S_u$ ,  $b$ , and  $R$ . Fig. 7a shows the variation of  $S/S_y$  with the increase of the loading step in uniaxial tension ( $S$  is the slip value). Fig. 7b shows the variation of the tensile stress with the increase of the slip value  $S$  for HRB400 steel bars reinforced C35 concrete and PVA fiber-reinforced concrete. The diameters of HRB400 steel bars are 14 mm and 20 mm, respectively. Before yielding, the slip of the reinforcement increases very slowly and the slip values are small. After yielding, the slip of the reinforcement increased rapidly, while the stress basically did not increase and the slip is very significant. This is also consistent with the phenomenon that the degradation rate of the bond between the reinforcement steel and the concrete (or FRC) gradually increases after the concrete or FRC has gone through the stages of cracking and crushing in the test. Under the same stress conditions, the slip value of the reinforcement with a greater diameter is large and its bond-slip effect is more significant, which is consistent with the findings in reference (Cao et al., 2016).



(a) Unidirectional tension loading path

### 2.2.2 Finite-Element Model of Prefabricated BCJs

Displacement-based non-linear beam-column elements are applied to simulate precast beam or precast column elements, and together with the fiber model in OpenSees software. Beam-column joint element consists of three components, used to simulate different damage behaviors at BCJs, as shown in Fig. 8. The shear panel component is used to simulate the shear behavior of the joint, i.e., the stiffness and strength degradation under shear damage in the core zone of the joint. Eight bar-slip spring elements are used to simulate the strength and stiffness degradation of the joint. Four interface-shear springs are applied to simulate the degradation of shear transfer capacity at the joint interface. The constitutive model of the shear panel is Pinching4 model, as shown in Fig. 9. In Fig. 9,

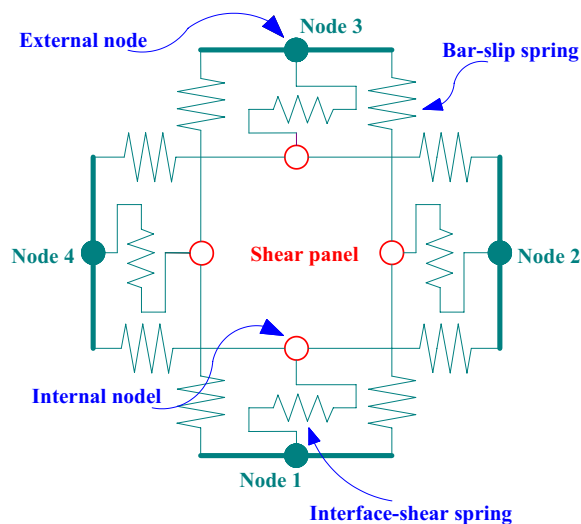
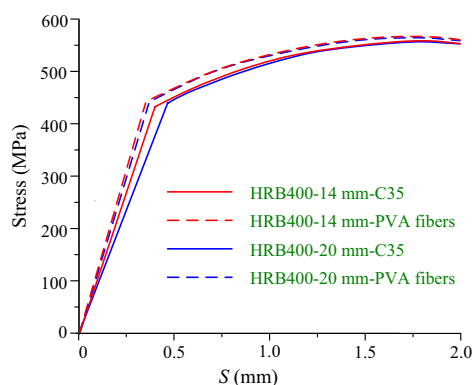
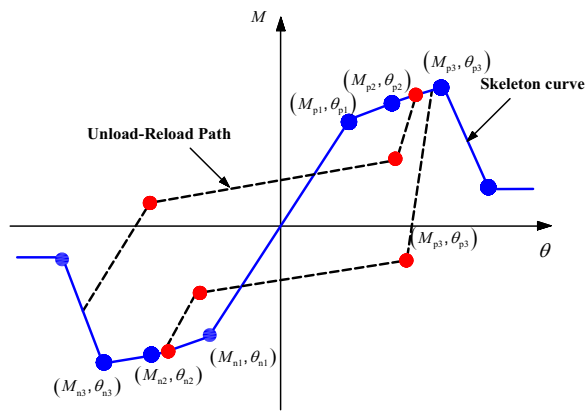


Fig. 8 Beam-column joint element



(b) Stress-strain slip curves

Fig. 7 Stress-slip curves of HRB400 reinforcement in uniaxial tension



**Fig. 9** Pinching4 model

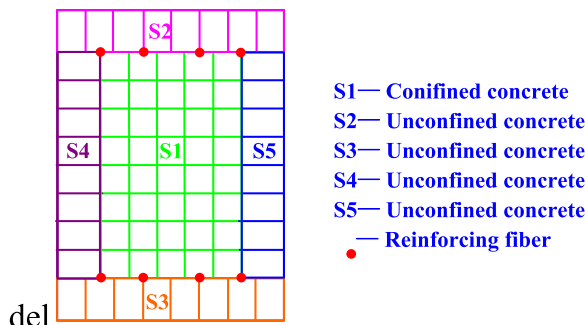


**Fig. 10** Cross section of the fiber model

$M_{pi}$  and  $M_{ni}$  ( $i = 1, 2, 3$ ) are the bending moments;  $\theta_{pi}$  and  $\theta_{ni}$  ( $i = 1, 2, 3$ ) are the drift ratios. It can accurately simulate the strength and stiffness degradation, and pinching effect of the prefabricated BCJs. The key to defining Pinching4 model is to define 16 parameters for the eight characteristic points of the skeleton curve envelope in the positive and negative directions, 6 key parameters for the unloading–reloading path, and stiffness and strength degradation criteria. The interfacial shear spring (interface-shear) is defined as an elastic material, and no degradation of the shear transfer is considered.

The fiber model is used for establishing the finite model, as shown in Fig. 10. It is proposed to show the pinching effect on the hysteretic behavior of precast-reinforced columns and precast beams by considering the bond-slip effect. During the tests, it was observed that the grouted sleeve connection remained undamaged (Sun et al., 2023a, 2023b). Hence, the equivalent area method is used to consider the influence of the grouted sleeve. The grouted sleeve fiber is converted to an equivalent steel rebar based on the area equivalence principle according to the AASHTO guide (Culmo et al., 2018). In Fig. 10, S1 area represents the core concrete, i.e. the

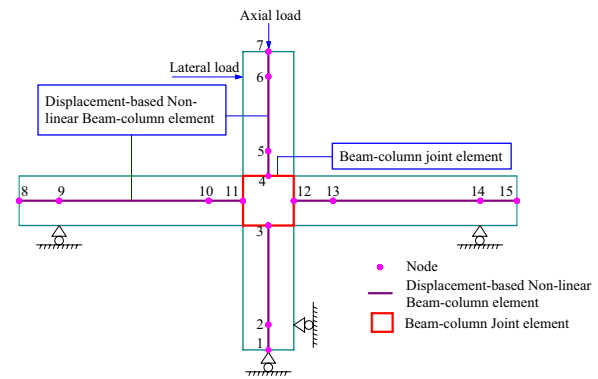


**Fig. 11** Schematic diagram of the finite-element model of prefabricated BCJs

**Table 6** Lateral load loading mode of prefabricated BCJs

Loading level	Drift ratio (%)	Displacement (mm)	Number of cycle
1	0.10	1.50	3
2	0.30	4.50	3
3	0.50	7.50	3
4	0.75	11.25	3
5	1.00	15.00	3
6	1.50	22.50	3
7	2.00	30.00	3
8	2.75	41.25	3
9	3.50	52.50	3

confined concrete area. S2, S3, S4 and S5 areas outside the confined concrete area represent the unconfined concrete area. The finite model consists of four fiber column elements, six fiber beam elements, and one beam–column joint element. The finite model is established in OpenSees Software, as described in Fig. 11. Five fiber column elements are established (nodes 1–6). Six fiber beam elements are established (nodes 8–15). Beam–column joint elements are established between nodes 3, 4, 10 and 11 to simulate the reinforcing bond-slip and shear behavior in the core zone of the joint. The fiber model of the prefabricated BCJ is loaded using the lateral drift ratio loading mode as the experimental loading mode in reference (Sun et al., 2023a). The lateral drift ratios are set in Table 6. Each drift ratio is loaded three cycles.

### 3 Numerical Results and Discussion on the Seismic Performance

#### 3.1 Hysteresis Curves of Prefabricated BCJs

Due to the experimental hysteresis, curves in reference (Sun et al., 2023b) were affected by various factors, the measured hysteresis curves in the positive and negative loading directions performed asymmetric characteristics,

while the numerical models are established without distinguishing the loading directions. Therefore, the experimental hysteresis curves of specimen PFRC1 from reference (Sun et al., 2023b) are moderately shifted to compare the accuracy of the finite-element models, which has no effect on the calculation of the relevant seismic behavior indexes.

The numerical simulation and test hysteresis curves of the three prefabricated BCJs are compared, as described in Fig. 12. Due to some errors in the fabrication and loading of the specimens from the reference (Sun et al., 2023a), the hysteresis curves obtained from the tests showed some differences in the seismic performance in the positive and negative directions, while the differences in the simulated results were smaller. The simulated hysteresis curves are almost close to those obtained from the test, reflecting the simulated loading–unloading paths and directions, the selected element types and material constitutive models can better reflect the shear effect and reinforcement bond-slip effect. In the late stage of displacement amplitude loading, the simulated load decreases more slowly than the experimental results

because the finite-element model considers the bond slip of reinforcement. The shapes of the hysteresis curves of the three prefabricated FRC BCJs are fuller than those of specimen PRC1. The hysteresis curves of specimens PFRC1 and PFRC2 almost coincide, indicating that adding PVA fibers can reduce or even eliminate the use of stirrups. In general, the simulated hysteresis curves are developed using the polyline model, taking into account the computational efficiency, the overall pinch phenomenon, stress–strain characteristic points matched well with the overall trend. Coupled with the inherent randomness of the tests due to concrete variability and processing level limitations, the simulated results are sufficient for seismic analysis and corresponding extended analysis of prefabricated BCJs.

### 3.2 Skeleton Curves of Prefabricated BCJs

Fig. 13 shows the test and numerical simulation skeleton curves of the prefabricated BCJs. Since there is some error in the fabrication and loading of the specimens, the test skeleton curves have some differences in the seismic performance in the positive and negative directions.

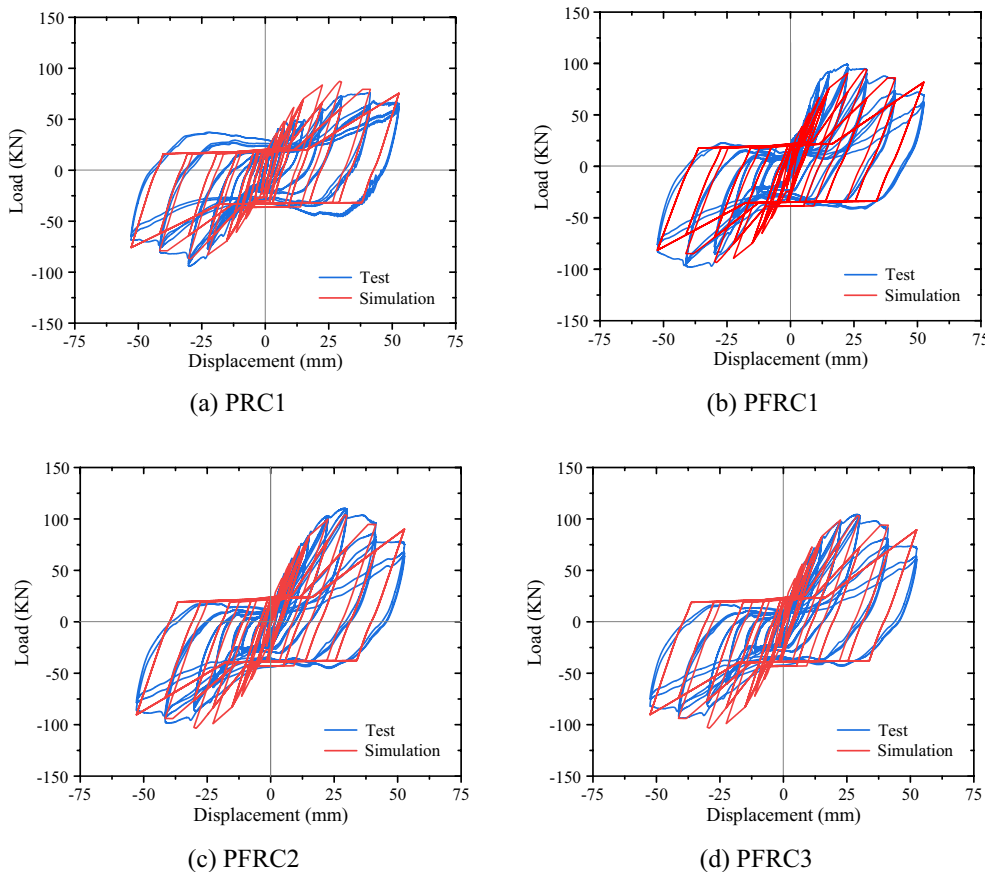


**Fig. 12** Hysteresis curves of prefabricated BCJs

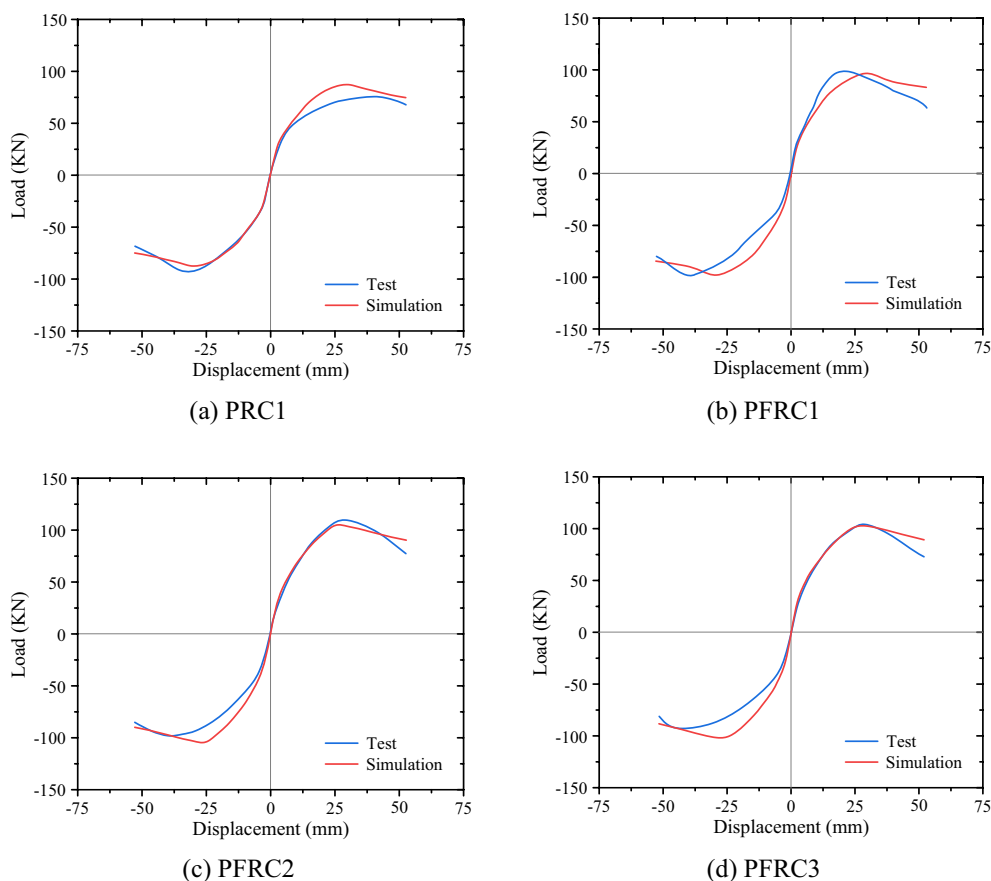


**Fig. 13** Skeleton curves of prefabricated BCJs

The numerical simulation and test skeleton curves of the prefabricated BCJ basically overlap in the rising section. During positive loading, the simulated and experimental skeleton curves of specimens PFRC2 and PFRC3 basically overlap. During negative loading, the simulated accuracy of specimens PRC1 is high. The skeleton curves of specimens PRC1 declined relatively gently. The bearing capacity of the three precast specimens reinforced with fibers was significantly higher than that of specimen PRC1. The core zone of specimen PFRC2 was not equipped with stirrups. The simulated skeleton curves of specimen PFRC2 was basically consistent with that of specimen PFRC1, indicating that the bearing capacity of the specimen using FRC in the core zone of the joint were less affected by the stirrups.

### 3.3 Bearing Capacity and Ductility of Prefabricated BCJs

The simulated yield points of the prefabricated BCJs are calculated using the energy area method in reference (Park, 1989), which is the same as the experimental yield point calculation method in reference (Sun et al., 2023a). From Tables 7 and 8, it can be found that the simulated

relative errors of the bearing capacity are below 15%. The simulated relative errors of the ductility coefficients of specimen PRC1 is -17.6%, while those of the three prefabricated FRC BCJs are below 5%. The numerical results indicate that the established fiber models have a high precision for simulating the bearing capacity and displacement ductility of prefabricated FRC BCJs with grouted sleeves connections.

The simulated bearing capacity of the three prefabricated FRC BCJs is greater about 15% than that of specimen PRC1. The simulated displacement ductility coefficients of the three prefabricated FRC BCJs are greater about 20% than that of specimen PRC1. Therefore, the addition of PVA and steel fibers in the core zone of the joint can greatly improve the bearing capacity of prefabricated BCJs and have a great influence on the displacement ductility of prefabricated BCJs. The simulated bearing capacity and displacement ductility coefficients of specimens PFRC1 and PFRC2 are almost the same, indicating that FRC in the core zone of the joint can improve the bearing capacity and displacement ductility of prefabricated BCJs without equipped with stirrups.

**Table 7** Test and numerical simulation bearing capacity and displacement ductility coefficients

Specimen no	Test result					Numerical simulation result				
	$F_y$ (kN)	$F_u$ (kN)	$\Delta_y$ (mm)	$\Delta_u$ (mm)	$\mu$	$F_{y,c}$ (kN)	$F_{u,c}$ (kN)	$\Delta_{y,c}$ (mm)	$\Delta_{u,c}$ (mm)	$\mu_c$
PRC1	67.02	84.58	21.22	44.55	2.10	73.70	86.70	20.90	51.17	2.47
PFRC1	75.75	86.99	15.71	50.22	3.20	82.09	84.83	16.54	52.26	3.16
PFRC2	75.81	85.98	15.64	47.29	3.02	86.10	87.79	16.57	52.25	3.15
PFRC3	77.52	88.38	16.18	51.09	3.16	86.09	88.79	16.60	52.44	3.16

Note:  $\Delta_y$  and  $\Delta_u$  indicate the test displacements at the test yield load  $F_y$  and maximum load  $F_u$ , respectively (Sun et al., 2023a; Zhuang et al., 2022b);  $\Delta_{y,c}$  and  $\Delta_{u,c}$  indicate the numerical displacements at the numerical yield load  $F_{y,c}$  and maximum load  $F_{u,c}$ , respectively;  $\mu$  is the test ductility coefficient, and  $\mu_c = \Delta_{u,c} / \Delta_{y,c}$  is the numerical ductility coefficient, and  $\mu_c = \Delta_{u,c} / \Delta_{y,c}$

**Table 8** Numerical accuracy of bearing capacity and displacement ductility coefficients

Specimen No	$F_{y,c}$ %	$F_{u,c}$ %	$\Delta_{y,c}$ %	$\Delta_{u,c}$ %	$\mu_c$ %
PRC1	9.97	2.50	-13.80	-1.50	-17.62
PFRC1	13.65	0.81	5.28	4.06	-1.25
PFRC2	13.57	2.00	5.95	10.49	4.30
PFRC3	11.05	0.46	2.97	2.60	0

**3.4 Energy Dissipation Curves of Prefabricated BCJs**

Fig. 14 describes a comparison of test and numerical simulation normalized cumulative hysteretic energy coefficient  $E_N$  of the prefabricated specimens, which is calculated using the same method as in reference (Sun et al., 2023a). The simulated and experimental total cumulative hysteretic energy-dissipation of the three prefabricated BCJs is calculated in Table 9. At the initial loading

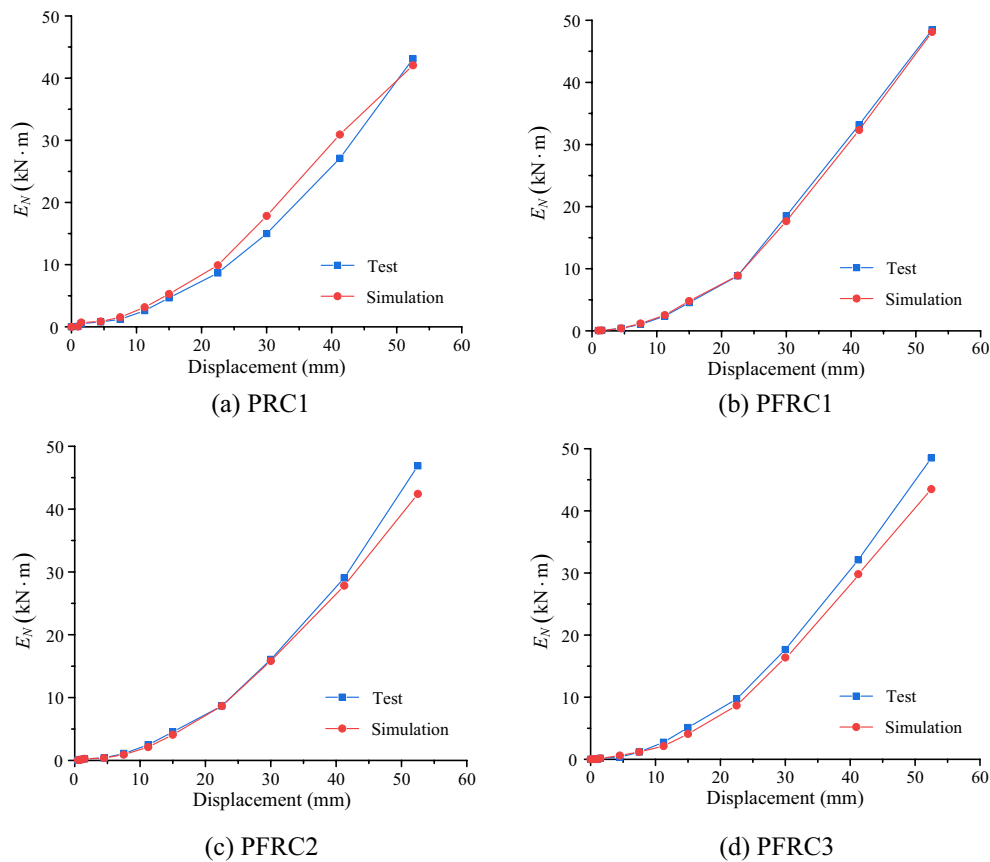


**Fig. 14** Cumulative energy-dissipation curves of prefabricated BCJs

**Table 9** Numerical results and accuracy of the total cumulative hysteretic energy-dissipation

Specimen No	Test value $T$ (kN · m)	Numerical simulation value $S$ (kN · m)	Relative error $((S-T) / T) \%$
PRC1	43.11	42.06	- 2.44
PFRC1	48.45	48.11	- 0.7
PFRC2	46.90	42.41	- 9.57
PFRC3	48.52	43.49	- 10.37

stage, the simulated and experimental curves almost overlap, but there are differences between the simulated and experimental curves at the middle and last loading stages. At the last loading displacement, the increase of the simulated total cumulative energy-dissipation of each specimen is smaller than the experimental result. The simulated and experimental curves of specimen PFRC1 almost overlap. The simulated total cumulative energy-dissipation of specimen PFRC1 is larger than that of specimen PFRC2, indicating that the prefabricated FRC specimen without stirrups in the core zone of joint can

get good energy dissipation capacity. The simulated total cumulative energy-dissipation of each prefabricated specimen is relatively close to the experimental result with a maximum relative error of less than 11%.

**3.5 Stiffness Degradation Curves of Prefabricated BCJs**

The simulated average loop stiffness  $K$  (Zhuang et al., 2022b) is used to measure the stiffness degradation of the prefabricated BCJs. The experimental and numerical simulation stiffness degradation curves of the three prefabricated BCJs are compared, as described in Fig. 15. The simulated initial stiffness is greater than the experimental one. After the first 6 cycles of loading, the simulated average loop stiffness curve is very close to the experimental stiffness. The stiffness degradation of each specimen is first fast and then slow. In the later stages of loading, the stiffness of each specimen is very low, indicating a high degree of damage to the specimen. The initial stiffness of specimen PFRC1 is almost equal to that of specimen PFRC2, and the degradation rates of the two specimens are also almost equal, indicating that with or without stirrups in the core zone of prefabricated joints has a very small effect on the stiffness degradation. The stiffness

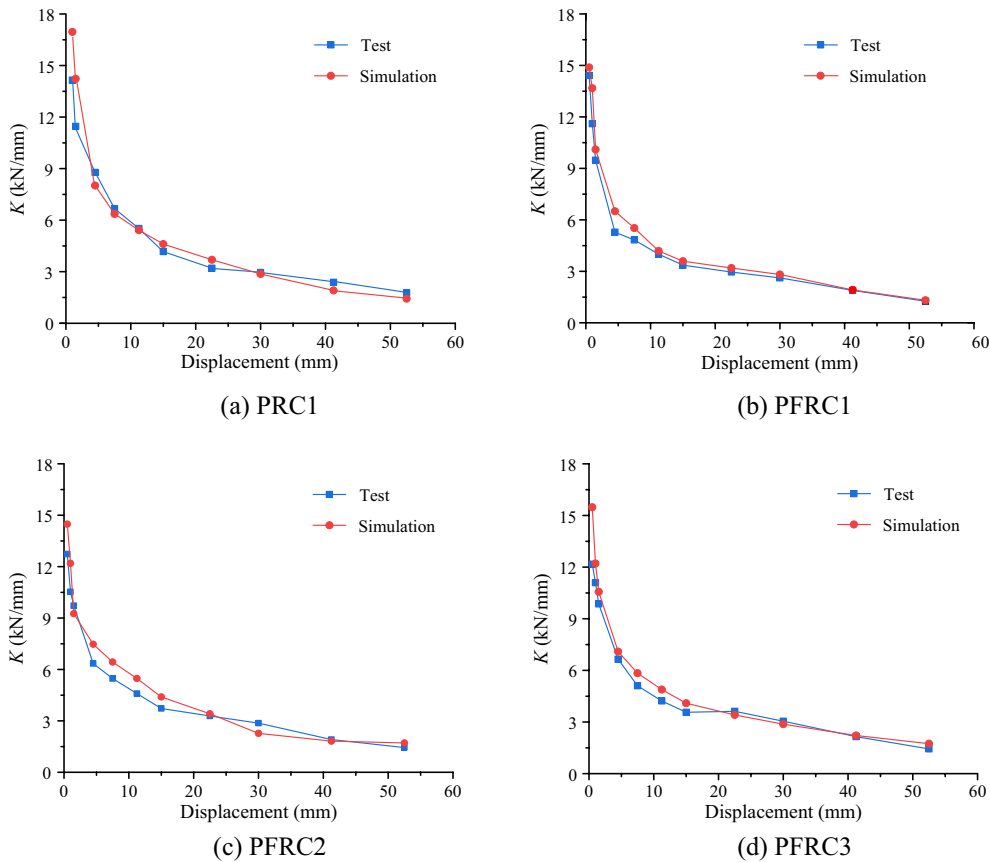


**Fig. 15** Stiffness degradation curves of prefabricated BCJs

degradation of specimens PFRC1 is almost the same with of specimen PFRC2. FRC can provide large stiffness in the early deformation stage, while in the large deformation stage, the stiffness provided by fiber-reinforced concrete was not enough to make up for the defects in the anchorage or grouted sleeve connections.

#### 4 Parametric Analysis of Effect Factors on the Seismic Behaviors Of Prefabricated FRC BCJs

##### 4.1 Effect of Axial Load Ratio on Prefabricated FRC BCJs

Due to limited experimental data, the effect of axial load ratio ( $n$ ) on some seismic performance indexes of prefabricated FRC BCJs with grouted sleeve connections is further investigated numerically. The column and beam cross-sectional dimension, shear-to-span ratio, fiber volume content and reinforcement of specimen PFRC3 are kept constant by varying its axial load ratio ( $n$ ) only from 0.15 to 0.6. The effect of  $n$  on the seismic behavior of the prefabricated FRC BCJ is described in Fig. 16. As  $n$  increases from 0.15 to 0.6, the hysteresis curve and skeleton curve of the prefabricated FRC BCJs almost overlap, indicating that increase of the axial load has no effect on

the hysteresis curve and skeleton curve of the prefabricated FRC BCJs. As  $n$  increases from 0.15 to 0.6, the stiffness degradation rates of the prefabricated FRC BCJs are almost the same. As  $n$  increases from 0.15 to 0.6, the peak load of the prefabricated FRC BCJs increases from 103.28 kN to 112.60 kN, with an increase of 9.02%. When  $n$  is not greater than 0.45, the bearing capacity of prefabricated FRC BCJs increases; when  $n$  is greater than 0.45, the bearing capacity of prefabricated FRC BCJs is almost unchanged. From above analysis, it can be found that the effect of  $n$  on the seismic behavior of prefabricated FRC BCJs can be negligible in the case that the prefabricated FRC BCJs has a moderate value of shear-to-span.

##### 4.2 Effect of Shear-to-Span Ratio on Prefabricated FRC BCJs

The column and beam cross-sectional dimension, axial load ratio, fiber volume content and reinforcement of specimen PFRC3 are kept constant by varying its shear-to-span ratio ( $s$ ) only from 2 to 3.5. The effect of  $s$  on the seismic behavior of the prefabricated FRC BCJs with grouted sleeve connections is described in Fig. 17. As  $s$  increases from 2 to 3.5, the hysteresis curve and skeleton

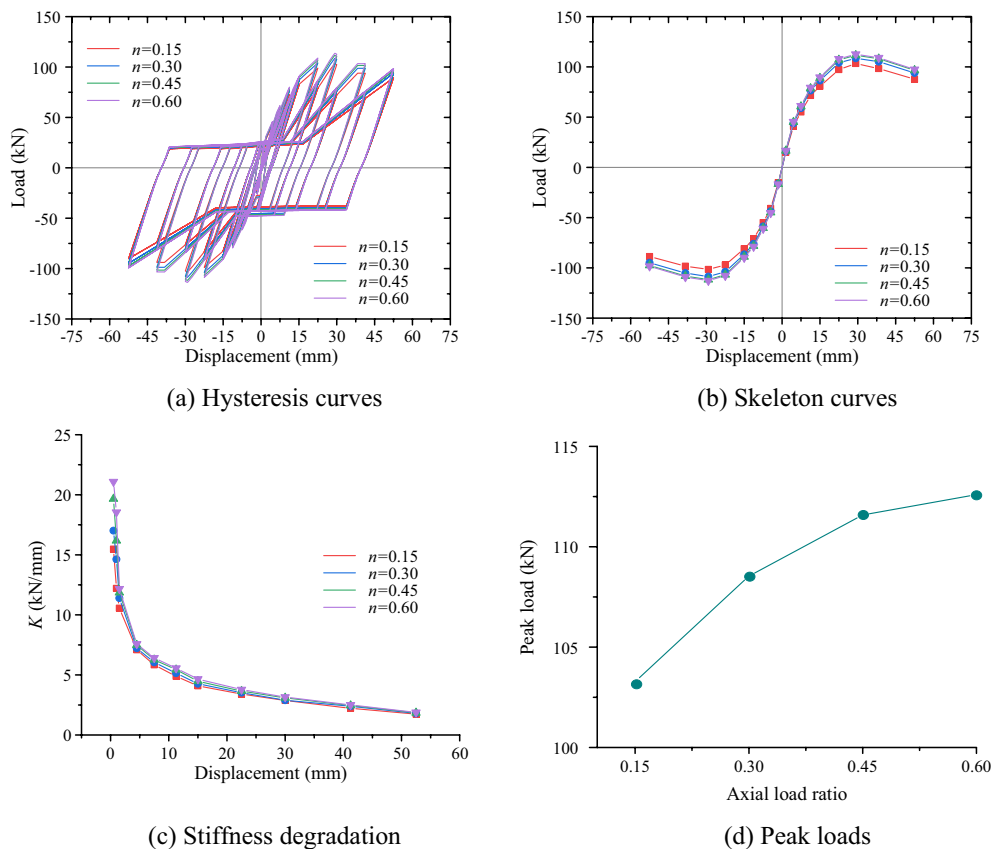


**Fig. 16** Effect of axial load ratio on prefabricated FRC BCJs

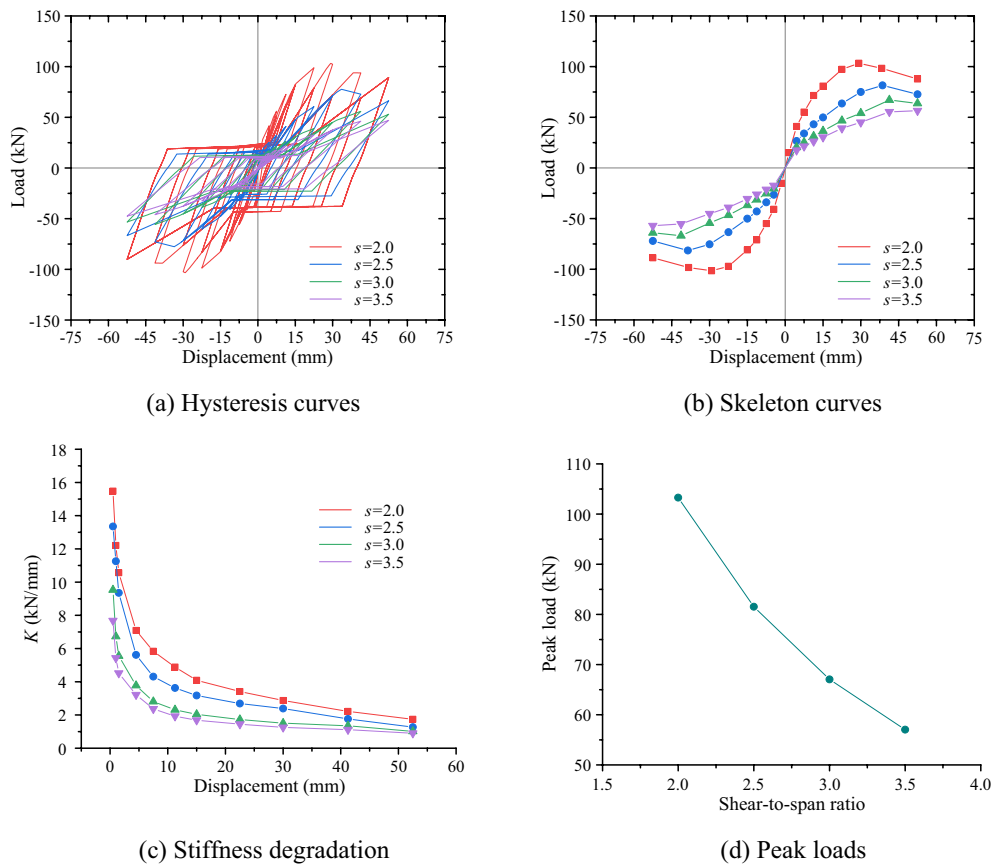


**Fig. 17** Effect of shear-to-span ratio on prefabricated FRC BCJ specimens

**Table 10** Numerical results and accuracy of the total cumulative hysteretic energy-dissipation

$\lambda$	$F_{yc}$ (kN)	$\Delta_{yc}$ (mm)	$F_{mc}$ (kN)	$\Delta_{uc}$ (mm)	$\mu_c$
2.0	86.10	16.57	103.28	52.25	3.15
2.5	67.92	17.38	81.53	52.50	3.02
3.0	51.81	21.29	67.04	52.50	2.47
3.5	46.12	24.53	57.04	52.50	2.14

curve change very significantly. The stiffness degradation curve varies greatly. At the same loading displacement, the stiffness degradation rate of the prefabricated FRC BCJs becomes smaller and smaller. The initial stiffness of the prefabricated FRC BCJs also becomes smaller and smaller. The peak load of the prefabricated FRC BCJs decreases from 103.28 kN to 57.04 kN, with an decrease of 44.77%. The simulated bearing capacity and displacement ductility coefficients of prefabricated FRC BCJs are shown in Table 10. It can be found that the bearing capacity and displacement ductility coefficients of PBCJs-CM gradually decrease as  $s$  increases. When  $s$  is greater

than 2.5, the ductility coefficient of PBCJs-CM is greater than 3.0. Therefore, it is recommended that the optimum range of  $s$  for prefabricated FRC BCJs is 2.0–2.5.

### 5 Conclusions

In present study, the seismic performance of prefabricated FRC BCJs is investigated numerically. The following conclusions are obtained.

(1) The Concrete02 material model and Reinforcing Steel material model can accurately simulate the constitutive relationship of concrete and reinforcing steel, respectively. The beam–column joint elements can accurately simulate different damage behaviors of the joint zone. The Bond\_SP01 material model can accurately simulate the bond-slip between the reinforcing steel, concrete, and grouted sleeve connections.

(2) The simulated hysteresis curves and skeleton curves of prefabricated BCJ specimens are similar to the experimental results. The simulated seismic performance indexes such as bearing capacity, displacement ductility, energy-dissipation capacity and stiffness degradation are not much different from the experimental results with a relative error of about 15%.

(3) PVA and steel FRC have a great effect on improving the seismic behavior of prefabricated BCJs with grouted sleeve connections. Compared with the PVA FRC BCJs, the simulated bearing capacity of steel FRC BCJs improves more greatly.

(4) It is recommended that the optimum value of shear-to-span ratio for prefabricated FRC BCJs is 2.0–2.5. The effect of axial load ratio on the seismic behavior of PBCJs-CM is very small, and can be negligible in the case that the prefabricated FRC BCJs has a moderate value of shear-to-span ratio.

#### Acknowledgements

This research has been supported by China Scholarship Council; the Natural Science Research Project of Jiangsu Province Colleges and Universities (21KJD560002), China; Suqian Natural Science Foundation Project (K202012), China; Project funded by the research and innovation team of engineering structure seismic technology of Suqian University in 2020, China; Suqian City Guiding Science and Technology Plan Project (Z2020137), China; Research and Innovation Team Project of Suqian College (2021TD04), China; and the Fifth Provincial Research Funding Project of "333 High-level Talent Training" in 2020 (BRA2020241), China.

#### Author contributions

Mei-Ling Zhuang contributed to conceptualization, formal analysis, investigation, and writing. Jinsheng Chen and Dongsong Fei contributed to funding acquisition, numerical analysis and writing-review. Chuanzhi Sun contributed to funding acquisition, project administration, supervision, validation, project administration, writing-review and editing. Zhenbo Wang and Baodong Chen was involved in formal analysis and methodology. Qiao Yan was involved in formal analysis and methodology and project administration. All the authors read and approved the final manuscript.

#### Availability of data and materials

The data and materials used to support the findings of this study are available from the corresponding author upon request.

#### Declarations

#### Ethics approval and consent to participate

Not applicable.

#### Consent for publication

All the authors agree that the article will be published after acceptance.

#### Informed consent

Informed consent was obtained from all individual participants included in this study.

#### Competing interests

The authors declare that they have no competing interests.

Received: 7 October 2023 Accepted: 17 February 2024

Published online: 06 May 2024

#### References

- Cao, W. L., Liu, X., Liu, Q. Y., Tian, Z., & Lin, D. C. (2016). Experimental study on bond slip behavior of ordinary and high strength recycled concrete and steel bars. *Journal of Building Structures*, 37(52), 127–134.
- Chang GA, Mander JB. (1994). Seismic energy based fatigue damage analysis of bridge columns: Part 1: Evaluation of seismic capacity. Technical Report, 1994.
- Coffin, L. F., Jr. (1954). A study of the effects of cyclic thermal stresses on a ductile metal. *Technical Report Archive and Image Library*, 76, 931–950.
- Culmo, M. P., Marsh, L., Stanton, J., & Mertz, D. (2018). *Recommended AASHTO guide specifications for ABC design and construction*. Washington, D.C.: Transportation Research Board.
- Dangwal, S., & Singh, H. (2023). Seismic performance of corroded non-seismically and seismically detailed RC beam-column joints rehabilitated with High Strength Fiber Reinforced Concrete. *Engineering Structures*, 291, 116481.
- Eligehausen, R., Popov, E. P., & Bertero, V. V. (1982). *Local bond stress-slip relationships of deformed bars under generalized excitations*. EERC Report. Berkeley: University of California.
- Fischer, G., & Li, V. C. (2002). Effect of matrix ductility on deformation behavior of steel-reinforced ECC flexural members under reversed cyclic loading conditions. *ACI Structural Journal*, 99(6), 781–790.
- Gencturk, B., Elnashai, A. S., Lepech, M. D., & Billington, S. (2013). Behavior of concrete and ECC structures under simulated earthquake motion. *Journal of Structural Engineering*, 139(3), 389–399.
- Girgin, S. C., Misir, I. S., & Kahraman, S. (2017). Experimental cyclic behavior of prefabricated hybrid beam-column connections with welded components. *International Journal of Concrete Structures and Materials*, 11(2), 229–245.
- Gomes, A., & Appleton, J. (1997). Nonlinear cyclic stress-strain relationship of reinforcing bars including buckling. *Engineering Structures*, 19(10), 822–826.
- Guan, D., Guo, Z., Xiao, Q., & Zheng, Y. (2019). Experimental study of a new beam-column connection for prefabricated concrete frames under reversal cyclic loading. *Advances in Structural Engineering*, 19(3), 529–545.
- Gul, M. A. A., Khan, S. W., Ishag, M., Khan, F. A., Shahzada, K., & Gul, M. S. A. (2023). Structural behaviour of RC-ECC beam-column connections under quasi-static loading. *Materials Today Communications*, 35, 105763.
- Hawkins, N. M., Lin, I. J., & Jeang, F. L. (1982). Local bond strength of concrete for cyclic reversed loadings. In P. Bartos (Ed.), *Bond in Concrete* (pp. 151–161). London: Applied Science Publishers Ltd.
- Kurama, Y. C., Sritharan, S., Fleischman, R. B., Restrepo, J. I., Henry, R. S., Cleland, N. M., et al. (2018). Seismic-resistant prefabricated concrete structures: State of the art. *Journal of Structural Engineering*, 144(4), 03118001.
- Li, D.-b, Chai, Y.-k, Li, W.-l, & Xiang, R. (2022). Xiang. Experimental study and finite element analysis of seismic behaviour of novel prefabricated prestressed concrete frames. *Structure*, 38, 402–415.
- Lowes, L. N., & Altoontash, A. (2003). Modeling reinforced concrete beam-column joints subjected to cyclic loading. *Journal of Structural Engineering*, 129(12), 1686–1697.
- Maekawa, K., & Dhakal, R. P. (2002). Modeling for Postyield buckling of reinforcement. *Journal of Structural Engineering*, 128(9), 1139–1147.
- Manson, S. S. (1953). Behavior of materials under conditions of thermal stress. *Technical Report Archive and Image Library*, s3–4, 661–665.
- Ministry of Housing and Urban-Rural Development of Jiangsu Province. Technical specification for assembled monolithic concrete structure: DBJ61/T 87–2014. (2014). China Building Materials Industry Press, Nanjing.
- Ministry of Housing and Urban-Rural Development of Jiangsu Province. (2017). *Technical specification for framed structures comprised of prefabricated concrete components: DGJ32/TJ219-2017*. Jiangsu Phoenix Science and Technology Publishing House.
- Mitra, N. (2007). *An analytical study of reinforced concrete beam-column joint behavior under seismic loading*. University of Washington.
- MOHURD (Ministry of Housing and Urban-Rural Development of the People's Republic of China). (2014a). *Technical specification for prefabricated concrete structures: JGJ 1–2014*. China Architecture & Building Press.
- MOHURD (Ministry of Housing and Urban-Rural Development of the People's Republic of China). (2014b). *Technical specification for framed structures comprised of prefabricated prestressed concrete components: JGJ 224–2010*. China Architecture & Building Press.
- Nadir, W., Ali, A. Y., & Kadhim, M. M. (2021). Structural behavior of hybrid reinforced concrete beam-column joints under cyclic load: State of the art review. *Case Studies in Construction Materials*, 15, e00707.
- Noushini, A., Samali, B., & Vessalas, K. (2013). Effect of polyvinyl alcohol (PVA) fiber on dynamic and material properties of fiber reinforced concrete. *Construction and Building Materials*, 49(2), 374–383.

- Noushini, A., Samali, B., & Vessalas, K. (2015). Ductility and damping characteristics of polyvinyl-alcohol fiber reinforced concrete beam elements. *Advances in Structural Engineering*, 18(11), 1763–1788.
- Pantazopoulou, S. J., & Bonacci, J. F. (1994). On earthquake-resistant reinforced concrete frame connections. *Canadian Journal of Civil Engineering*, 21(2), 307–328.
- Parastesh, H., Hajjarasouliha, I., & Ramezani, R. (2014). A new ductile moment-restoring connection for prefabricated concrete frames in seismic regions: An experimental investigation. *Engineering Structures*, 70, 144–157.
- Park, R. (1989). Valuation of ductility of structures and structural assemblages from laboratory testing. *Bulletin of the New Zealand National Society for Earthquake Engineering*, 22(3), 155–166.
- Parra-Montesinos, G. J., & Chopreda, P. (2017). Deformation capacity and shear strength of fiber-reinforced cement composite flexural members subjected to displacement reversals. *Journal of Structural Engineering*, 133(3), 421–431.
- Paudel, S., Tanapornraweekit, G., & Tangtermsirikul, S. (2022). Numerical study on seismic performance improvement of composite wide beam-column interior joints. *Journal of Building Engineering*, 46, 103637.
- Paulay, T. (1989). Equilibrium criteria for reinforced concrete beam-column joints. *ACI Structural Journal*, 86(6), 635–643.
- Qian, H., Wang, X. Y., Xu, L., & Zhang, Y. Y. (2023). Experimental study on re-centering behavior and energy dissipation capacity of prefabricated concrete frame joints with shape memory alloy bars and engineered cementitious composites. *Engineering Structures*, 277, 115394.
- Saghafi, M. H., Golafshar, A., Zareian, M. S., & Mehri, A. H. (2021). Application of HPFRCC in beam-column joints to reduce transverse reinforcements. *Structures*, 31, 805–814.
- Said, S. H., & Razak, H. A. (2016). Structural behavior of RC engineered cementitious composite(ECC) exterior beam-column joints under reversed cyclic loading. *Construction & Building Materials*, 107, 226–234.
- Scott, B. D., Park, R., & Priestley, M. J. (1982). Stress-strain behavior of concrete confined by overlapping hoops at low and high strain rate. *Journal of the American Concrete Institute*, 70(1), 13–27.
- Sun, C. Z., Zhuang, M. L., Bai, L. T., Gao, L., Yu, C. R., Yang, J., Zhu, H. B., Qiao, Y., Shao, Y. F., & Zhang, W. H. (2023b). Experimental study on seismic behavior of novel precast concrete beam-column joints using mechanical connections. *Bulletin of Earthquake Engineering*, 21, 4429–4448.
- Sun, C. Z., Zhuang, M. L., Wang, Z. B., Chen, B. D., Gao, L., Qiao, Y., Zhu, H. B., Zhang, W. H., Yang, J., & Yu, C. R. (2023a). Experimental investigation on the seismic performance of prefabricated fiber-reinforced concrete beam-column joints using grouted sleeve connections. *Structural Concrete*. <https://doi.org/10.1002/suco.202200823>
- Suryanto, B., Tambusay, A., Suprobo, P., Bregoli, G., & Aitken, M. W. (2022). Seismic performance of exterior beam-column joints constructed with engineered cementitious composite: Comparison with ordinary and steel fibre reinforced concrete. *Engineering Structures*, 250, 113377.
- Xia, J., Chen, J. J., Shan, K. S., & Wu, Y. F. (2023). Seismic performance of corroded prefabricated column-footing joint with grouted splice sleeve connection: Experiment and simulation. *Journal of Building Engineering*, 80, 108112.
- Xia, J., Gan, R. L., Fang, Y., Zhao, Y. X., & Jin, W. L. (2020). Experimental study on direct shear performance of concrete-concrete interface of prefabricated structure sleeve grouting connection. *Journal of Zhejiang University (engineering Science)*, 54(3), 491–499.
- Xue, W., Hu, X., & Song, J. (2021). Experimental study on seismic behavior of prefabricated concrete beam-column joints using UHPC-based connections. *Structures*, 34, 4867–4881.
- Zhang, T. Y., Zhao, B. G., Li, R. G., & Du, X. Y. (2016). Monotonic and low cycle fatigue testing and research for HRB400 Steel. *Engineering Mechanics*, 33(4), 121–129.
- Zhao, J., & Sritharan, S. (2007). Modeling of Strain penetration effects in fiber-based analysis of reinforced concrete structures. *ACI Structural Journal*, 104(2), 133–141.
- Zhuang, M. L., Sun, C. Z., & Dong, B. (2022b). Experimental and numerical investigations on seismic performance of HTRB630 high-strength steel bars reinforced concrete columns. *Case Studies in Construction Materials*, 17, e01185.
- Zhuang, M. L., Sun, C. Z., Gao, L., Qiao, Y., Chen, J., Zhang, W. H., & Ma, Y. S. (2022a). Investigation on drift ratio limits of PVA fiber reinforced concrete

columns under different performance levels based on the Kunnath damage model. *Case Studies in Construction Materials*, 17, e01403.

## Publisher's Note

Springer Nature remains neutral with regard to jurisdictional claims in published maps and institutional affiliations.

**Mei-Ling Zhuang** is a lecturer of School of Transportation and Civil Engineering at Nantong University;

**Jinsheng Cheng** is an engineer at Suqian City Urban Construction Investment (Group) Co. Ltd.

**Dongsong Fei** is an engineer at Suqian City Urban Construction Investment (Group) Co. Ltd.

**Chuanzhi Sun** is a professor of School of Civil Engineering and Architecture at Suqian College;

**Zhenbo Wang** is a professor of College of Civil Engineering at Nanjing Tech University;

**Baodong Chen** is a student of College of Civil Engineering at Nanjing Tech University;

**Yan Qiao** is a professor of School of Civil Engineering and Architecture at Suqian College.